Catal Lett (2012) 142:50–59
DOI 10.1007/s10562-011-0725-9

Biobutanol Dehydrogenation to Butyraldehyde over Cu, Ru and Ru–Cu Supported Catalysts. Noble Metal Addition and Different Support Effects

J. Requies · M. B. Güemez · A. Iriondo · V. L. Barrio · J. F. Cambra · P. L. Arias

Received: 3 June 2011 / Accepted: 18 October 2011 / Published online: 5 November 2011

Abstract *n*-Butanol dehydrogenation to butyraldehyde was studied using Ru, Cu and Ru–Cu catalysts supported on ceria, titania and zirconia. Among the monometallic Cu and Ru supported catalysts, the non-noble catalytic systems recorded higher conversions and butyraldehyde selectivities than the noble catalysts. Furthermore, the $5Cu/ZrO_2$ catalyst had the best catalytic activity and selectivity. This behaviour is related to the good metal phase dispersion on the zirconia structure. The addition of Ru reduced this catalyst's performance because Ru incorporation weakened the Cu-support interaction and favoured the sintering of the Cu metal crystallites.

Keywords *n*-Butanol · Dehydrogenation · Cu · Ru · CeO_2 · TiO_2 · ZrO_2 · Butyraldehyde

1 Introduction

Aldehydes are important organic molecules for the synthesis of many different high value added products, such as acetals, plastics, perfume, etc. There is growing interest in renewable sources for all types of chemicals. Bioalcohols, such as ethanol, butanol or glycerol, can be produced from biomass and converted to their corresponding aldehydes, although appropriate processes are required for these conversions. The chemical industry produces aldehydes via alkene hydroformylation. Nevertheless, other processes such as bioalcohol catalytic dehydrogenation or catalytic oxidation reactions are chemical procedures that are more consistent with current environmental policies. Gas phase catalytic dehydrogenation has the advantage that the subsequent purification process is much simpler than in the case of partial oxidation. In partial oxidation processes, nitrogen dilutes the product flow when the reaction takes place with air.

Cu-based catalysts are the ones most widely used in dehydrogenation reactions, while Ru-based catalysts are commonly employed in oxidation reactions. In addition to this, there are few references in the literature to *n*-butanol dehydrogenation. Some of the reported studies were conducted using a very low partial pressure of alcohol. Shiau and Liaw [1, 2] reported high conversion and selectivity with copper–barium catalysts, while Raizada et al. [3] studied the influence of the zinc oxide catalyst preparation method on the catalytic activity for *n*-butanol dehydrogenation. In addition, Shiau and Tsai [4] found that SiO_2-supported Cu catalysts prepared by the electroless method recorded better activity and stability than those prepared by the impregnation method operating in gas phase and under atmospheric pressure. Similarly, Basinska et al. [5] also studied *n*-butanol conversion on iron oxide-supported Ru catalysts, which were prepared by different methods, and they concluded that a suitable procedure for metal deposition on the support leads to a higher selectivity toward the desired product.

Against this background, the main objective of this research was to study the production of butyraldehyde through *n*-butanol dehydrogenation. For this purpose, Cu, Ru and Ru–Cu catalysts supported on different oxides (ZrO_2, CeO_2 and TiO_2) were prepared, characterized and tested in *n*-butanol dehydrogenation.

J. Requies (✉) · M. B. Güemez · A. Iriondo · V. L. Barrio · J. F. Cambra · P. L. Arias
Department of Chemical and Environmental Engineering, School of Engineering, Bilbao, Spain
e-mail: jesus.requies@ehu.es

2 Experimental

2.1 Catalyst Preparation

The Ru, Cu and Ru–Cu catalysts were prepared by incipient wetness impregnation. The support materials used were ZrO_2, CeO_2 and TiO_2**.** ZrO_2 was obtained by the calcination of zirconium hydroxide, kindly provided by Eurosupport, The Netherlands; CeO_2 was obtained by the calcination of $Ce(NO_3)_3{\cdot}H_2O$ at 923 K for 4 h, (SigmaUltra >99.0%, Sigma–Aldrich); and titanium dioxide (Degussa, Aeroxide TiO_2 P25). $RuCl_3$ (Johnson Matthey, metallic base Ru 40%) and $Cu(NO_3)_2{\cdot}3H_2O$ (Alfa Caesar, 98%) were used as Ru and Cu precursors, respectively. The precursor solutions were prepared to achieve a nominal load of 5 wt% of Cu and 2 wt% of Ru. The suitable support amount was then contacted with the precursor solutions. After impregnation and drying, the samples were calcined in air using the following temperature programme:

$$313\,\mathrm{K} \xrightarrow{5(\mathrm{K/min})} 623\,\mathrm{K}\ (1\ \mathrm{h}) \xrightarrow{5(\mathrm{K/min})} 773\,\mathrm{K}\ (1\ \mathrm{h})$$

The monometallic catalysts were designed as follows: 5Cu/ZrO_2, 5Cu/TiO_2, 5Cu/CeO_2 and 2Ru/ZrO_2. The bimetallic catalyst, designed as 2Ru5Cu/ZrO_2, was developed by the impregnation of 5Cu/ZrO_2 catalyst. Their chemical composition is given in Table 1.

2.2 Catalysts Characterization

Different characterization techniques were used to determine the physical–chemical properties of the fresh and spent catalysts: inductively coupled plasma atomic emission spectroscopy (ICP-AES), N_2 adsorption–desorption isotherms at 77 K, temperature-programmed reduction (TPR), X-ray diffraction (XRD) and X-ray photoelectron spectroscopy (XPS).

2.2.1 ICP-AES

This technique was used to determine Ru and Cu metal contents. A Perkin-Elmer Optima 3300DV apparatus was used for the purpose. Solid samples were disaggregated in acid solutions (mixture of H_2SO_4, HF, and HNO_3).

2.2.2 N_2 Adsorption–Desorption Isotherms

The textural properties (BET surface areas and pore volumes and diameters) of the calcined catalysts were

Table 1 Metal loading determined by chemical analysis (ICP-AES), and XPS results for calcined and spent catalysts

Catalysts	B.E. (eV)				Surface atomic ratios		ICP-AES		TGA
	Ru $3d_{5/2}$	Cu $2p_{3/2}$	M 2p/3d	C 1s	Ru/M	Cu/M	Ru (wt%)	Cu (wt%)	C(g)//g) catalyst
Calcined									
5Cu/ZrO_2	–	934.0	182.2	–	–	0.114		6.18	
5Cu/CeO_2	–	933.9	882.6	–	–	0.331		4.73	
5Cu/TiO_2	–	933.9	458.6	–	–	0.270		5.40	
2Ru/5Cu/ZrO_2	281.0 (66) 282.9 (34)	934.2	182.1	–	0.097	0.185	0.98	5.85	
2Ru/ZrO_2	282.1 (61) 283.9 (39)	–	182.2	–	0.058	–	1.26		
Spent									
5Cu/ZrO_2	–	932.7	182.3	284.6 286.3–286.5 288.5–288.7	–	0.079			0.06
5Cu/CeO_2	–	932.7	882.6	284.6 286.3–286.5 288.5–288.7	–	0.268			0.01
5Cu/TiO_2	–	932.8	458.6	284.6 286.3–286.5 288.5–288.7	–	0.232			0.04
2Ru/5Cu/ZrO_2	280.0	932.8	182.2	284.6 286.3–286.5 288.5–288.7	0.068	0.118			0.09
2Ru/ZrO_2									0.02

B.E. binding energy and *M* supports (ZrO_2, CeO_2 or TiO_2)

evaluated by this technique, using a Micromeritics ASAP 2100 automatic device. Prior to characterization, the samples were degassed at 423 K for 24 h.

2.2.3 TPR

The reducible species, formed during the catalyst calcination step, and the reduction temperature were determined by this technique. The measurements were carried out using a Micromeritics TPD-TPR 2900 apparatus, equipped with a thermal conductivity detector. A continuous flow of 10% H_2/Ar (40 NmL/min) was passed over 200 mg of calcined catalyst powder. The temperature was increased from room temperature to 1233 K at a rate of 10 K/min. The sample was previously degassed at 523 K for 30 min.

2.2.4 XRD

XRD patterns were obtained using a Seifert XRD 3000P diffractometer, equipped with a PW 2200 Bragg–Brentano u/2u goniometer, bent graphite monochromator and automatic slit, using Cu Kα radiation ($\lambda = 0.15418$ nm) and 0.028° steps for scanning. The Scherrer equation was used to calculate the average particle size of the crystalline species.

2.2.5 XPS

This technique was used to evaluate the surface characteristics (oxidation state of the species formed, interactions, atomic ratios, etc.) of the samples. The measurements were carried out with a VG Escalab 200R spectrometer equipped with a hemispherical electron analyser and an Al Ka1 (h$\nu = 1486.6$ eV) 120 W X-ray source. The powdered samples were deposited on a stainless steel sample holder, placed in the pre-treatment chamber and degassed at 573 K. The base pressure of the spectrometer was typically 10^{-9} torr. The spectra were collected at a pass energy of 20 eV, which is typical of high resolution conditions. Both fresh and spent catalysts were analysed with this technique.

2.2.6 TGA-TPO

Temperature programmed oxidation analyses of spent catalysts were carried out using a thermogravimetric analyzer (Mettler Toledo TGA/SDTA 851e). The sample (20–30 mg) was heated from room temperature to 1173 K and the weight change was continuously monitored during heating in 100 mL/min of pure O_2 at a rate of 5 K/min.

2.2.7 Activity Tests

The activity tests were carried out in a bench-scale unit equipped with a tubular stainless steel reactor. The reactor was electrically heated in a furnace to the reaction temperature and the effluent stream was cooled to room temperature allowing gas/liquid separation. The catalyst (300 mg) was diluted with inert SiC ($m_{catalyst}/m_{SiC} = 1{:}9$ wt/wt) to avoid thermal gradients in the catalytic bed. The particle size range was 0.42–0.50 mm. Prior to reaction, the catalysts were reduced in situ with 100 NmL/min of 10 vol% H_2/N_2 mixture at 0.1 MPa of total pressure and 523 K for 2 h. The reduced catalysts were tested under the following conditions: 0.1 MPa of total pressure, 648 K and an *n*-butanol flow rate of 0.1 mL/min. The gas phase produced was analyzed on-line using a Micro GC Varian equipped with a high sensitivity TCD and three columns (Molecular Sieve, PoraPLOT Q and CP-4900). The liquid phase produced was analyzed offline by a GC (HP 6890) equipped with FID and TCD detectors, and a DB-Wax column. For a better understanding of catalytic activity and product distribution, the following parameters were calculated:

(i)

$$n\text{-butanol conversion } (\%) = \frac{n^{\text{Feed}}_{\text{BuOH}} - n^{\text{Out}}_{\text{BuOH}}(\text{mol/min})}{n^{\text{Feed}}_{\text{BuOH}}(\text{mol/min})} \times 100$$

(ii) $$\text{Yields} : Y_i\ (\%\ ) = \frac{n_i^{\text{out}}(''i'' \text{ liquid product mol/min})}{n_{\text{BuOH converted}}(\text{mol/min})} \times 100$$

3 Experimental Results

3.1 Characterization Results

3.1.1 Chemical Composition and Textural Properties

As can be seen in Table 1, the Cu contents are similar to the intended one (5% in the nominal weight) for Cu-based catalysts. Among the monometallic catalysts, the 5Cu/ZrO_2 catalyst has a higher metallic content than 5Cu/TiO_2 and 5Cu/CeO_2 catalysts, while the 5Cu/CeO_2 catalyst has the lowest Cu content, albeit quite similar to the nominal one. For the 2Ru/ZrO_2 catalyst, the Ru content was lower than the desired one. In the case of bimetallic catalysts, a slightly decrease was observed for both metals.

The textural properties (calculated using the BJH method) are summarized in Table 2. These data indicate that all the catalysts prepared are mainly mesoporous, like the bare supports. The ZrO_2 support has a large BET surface area as compared to CeO_2 and TiO_2 supports. This big specific area recorded by ZrO_2 support favours the deposition of higher amounts of Cu, as the data in Table 1 reveal. For the 5Cu/TiO_2 and 5Cu/CeO_2 catalysts, a similar area was measured after metal incorporation. According to

Table 2 Physical and textural properties of supports and catalysts

Sample	S_{BET}	Total pore volume	Micropore volume	Average pore diameter
Support				
ZrO_2	391.8	0.226	0.0960	23.1
CeO_2	57.4	0.098	0.0016	137.2
TiO_2	66.6	0.150	0.0380	87.8
Catalyst				
$5Cu/ZrO_2$	171.8	0.116	0.0220	42.3
$5Cu/CeO_2$	56.0	0.096	–	70.3
$5Cu/TiO_2$	59.2	0.138	0.0020	134.3
$2Ru/ZrO_2$	168.9	0.120	0.0100	44.8
$2Ru5Cu/ZrO_2$	161.6	0.113	0.0140	48.6

Units S_{BET} (m^2/g), Total pore and micropore volume (cm^3/g), Average pore diameter (Å)

the literature, this effect could be due to pore blockage by the metal [6]. Furthermore, these surface area data are in agreement with the pore and micropore volume diminution and the rise of the catalysts' average pore diameter (see Table 2) also observed.

For the ZrO_2 support, the addition of Cu or Ru causes a significant decrease in the BET surface area with a slightly higher average pore diameter. In comparison with $5Cu/ZrO_2$ and $5Cu/TiO_2$ catalysts, the $5Cu/CeO_2$ catalyst records a reduction in the average pore diameter possibly due to the incorporation of Cu species in the mesopores, as micropores are not seen to promote this effect.

3.1.2 TPR

The TPR profiles for the calcined catalysts are shown in Fig. 1. Two peaks at low temperatures are usually measured in the TPR profiles of Cu-supported catalysts. These peaks are typically linked to the presence of Cu with different oxidation states. The first peak (around 420 K) is attributed to the reduction of CuO to Cu_2O, while the second peak (around 460 K) is ascribed to the reduction of Cu_2O to Cu° [7, 8]. Therefore, the reduction of Cu species to metallic Cu takes place through Cu_2O formation. The reduction temperatures measured for $5Cu/ZrO_2$, and especially for $5Cu/TiO_2$, are higher than the ones measured for $5Cu/CeO_2$. This observation indicates that the interaction between Cu species and TiO_2 and ZrO_2 supports is higher than the one with CeO_2 support. Only the TPR profile of $5Cu/CeO_2$ catalyst showed two additional peaks at 709 and 1001 K, which can be attributed to the reduction of superficial and bulk CeO_2, respectively [7, 8].

For the $2Ru/ZrO_2$ catalyst, three reduction peaks were measured at 381, 423 and 447 K. These peaks probably correspond to the reduction of ruthenium oxides with different interactions with the support [9]. According to several authors [10, 11], Ru species would be mainly in the RuO_2 form for Ru-supported catalysts such as Ru/SiO_2, Ru/Al_2O_3, Ru/TiO_2 [10] and Ru/CeO_2 [12] after calcination. Hence, the same behaviour is expected for the $2Ru/ZrO_2$ catalyst prepared.

Regarding the TPR profiles of Ru–Cu bimetallic catalyst, three peaks were registered at 392, 436 and 461 K. The first peak corresponds to the reduction of Ru, while the

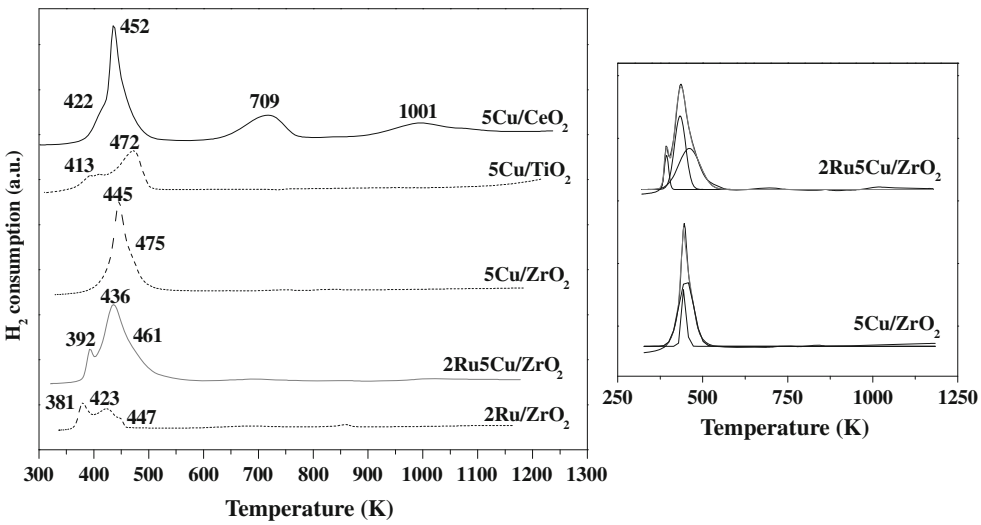

Fig. 1 TPR profiles of Cu and Ru catalysts supported on ZrO_2, CeO_2 and TiO_2 and profile deconvolution of the $2Ru5Cu/ZrO_2$ and $5Cu/ZrO_2$ catalysts

peaks registered at higher temperatures can be attributed to Cu species reduction. These last two peaks are shifted slightly more to lower temperatures than the ones where the same peaks appeared for the $5Cu/ZrO_2$ catalyst. This could be due to the hydrogen spillover effect favoured by the presence of a noble metal such as Ru [13]. These two peaks contain the contribution of the Ru reduction. The deconvolution of the $5Cu/ZrO_2$ and $2Ru5Cu/ZrO_2$ catalyst profiles (see Fig. 1) shows that the proportion of reducible Cu in the $5Cu/ZrO_2$ catalyst was 78.8%, while in the $2Ru5Cu/ZrO_2$ catalyst this proportion increases to 91.8%.

3.1.3 XRD

The XRD patterns show that the catalysts were formed by different crystal species. For the reduced $5Cu/CeO_2$ and $5Cu/TiO_2$ catalysts, reflexions were detected associated to Cu° (PDF 01-085-1326) and diffraction lines ascribed to cerianite type CeO_2 (PDF, powder diffraction file, 01-075-0151) and, anatase and rutile type TiO_2 (PDF 01-071-1166 and 01-075-1750, respectively) [14]. In the case of the reduced $5Cu/ZrO_2$ (Fig. 2) catalyst, only ZrO_2 reflexions (PDF 01-079-1771) were registered. These reflexions correspond to a cubic ZrO_2 structure. In addition, the absence of Cu° is indicative of a good dispersion of this Cu on the ZrO_2 support [15]. For the calcined catalyst, and apart from the ZrO_2 phase, diffraction lines attributed to CuO (PDF 00-041-0254) were detected (Fig. 2). The absence of diffraction lines of CuO for the reduced catalyst indicates this oxide was totally reduced to Cu°. Nevertheless, the spent $5Cu/ZrO_2$ catalyst showed a reflexion associated to Cu°. This observation suggests that Cu° suffers a sintering phenomenon during *n*-butanol dehydrogenation (Fig. 2).

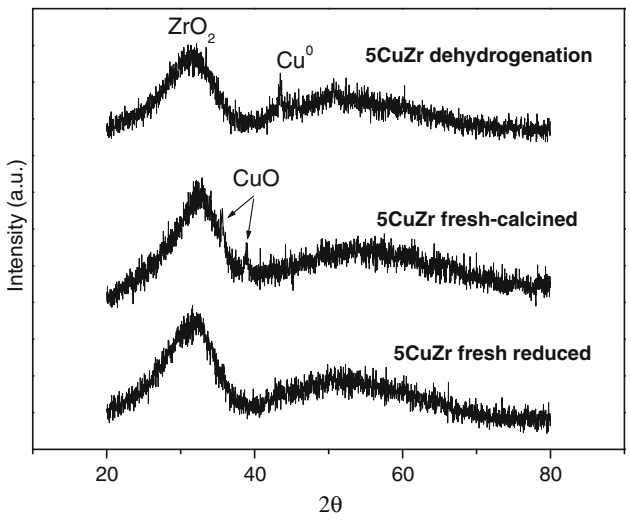

Fig. 2 XRD of the 5CuZr freshly reduced catalyst, freshly calcined catalyst, and after *n*-butanol dehydrogenation

Regarding the reduced $2Ru5Cu/ZrO_2$ catalyst, no reflexions of Ru and Cu phases were observed, suggesting a good dispersion of the metal phases [15].

The reduced $5Cu/CeO_2$ and $5Cu/TiO_2$ catalysts recorded an average particle size of 61 and 51.4 nm, respectively; hence their average particle sizes were higher than the one measured for the reduced $5Cu/ZrO_2$ catalyst. In fact, after the use of $5Cu/ZrO_2$ in the dehydrogenation reaction, the calculated average particle size was 29.8 nm lower than in the freshly reduced $5Cu/CeO_2$ and $5Cu/TiO_2$. The freshly reduced bimetallic catalyst also had a good Cu^0 dispersion, as its particles were below the detection level of the XRD technique.

3.1.4 XPS-TGA

The Cu 2p, Ru 3d, Ti 2p, Ce 3d, and Zr 3d core-levels of calcined and spent catalysts and the metal/support atomic surface ratios as determined by XPS are summarized in Table 1. For the calcined $5Cu/ZrO_2$, $5Cu/CeO_2$, $5Cu/TiO_2$ and $2Ru5Cu/ZrO_2$ catalysts, the binding energy of Cu $2p_{3/2}$ is close to the values 933.9–934.2 eV, which can be assigned to Cu^{2+} [16, 17] species. After the dehydrogenation reaction, this binding energy took values of around 932.7–932.8 eV. These values are typically assigned to Cu° species [16]. Regarding the supports, the Ce $3d_{5/2}$, the Zr 3d and the Ti 2p core-levels recorded values at 882.5–882.7 eV, associated to the presence of Ce^{4+} species (CeO_2) [18], at 181.7–182.1 eV, attributed to the ZrO_2 species [19], and at 458.6 eV, assigned to the Ti^{4+} species (TiO_2) [20]. These energy levels are similar for calcined and spent catalysts.

The Ru $3d_{5/2}$ energy level for monometallic and bimetallic Ru-supported catalysts was also analyzed. The calcined $2Ru/ZrO_2$ catalyst showed binding energies at around 281.7–282.6 and 282.6–283.3 eV attributed to RuO_3 [21, 22] and RuO_4 surface species [23], respectively. For the calcined $2Ru5Cu/ZrO_2$ catalyst, RuO_2 (280.7–281.0 eV) and RuO_4 (282.6–283.3 eV) species were registered [23]. After the dehydrogenation reaction, the bimetallic catalyst presented a binding energy at 280.0 eV attributed to Ru° surface species [21, 22].

In addition to this, three different peaks corresponding to C 1s core-level were registered for all used catalysts at 284.9 eV (C–C/C–H) [24], 286.3–286.5 eV (C–O) [25] and 288.5–288.7 eV (R–COO) [26]. These peaks could be assigned to surface carbon deposition during the reaction. To confirm these results, different TGA analyses were conducted. These spent catalysts were the ones featured in Fig. 4. The data derived from the TPO analysis of the spent catalysts are collected in Table 1. These data indicate that carbonaceous species were deposited on the catalysts under dehydrogenation conditions. By comparing the amount of

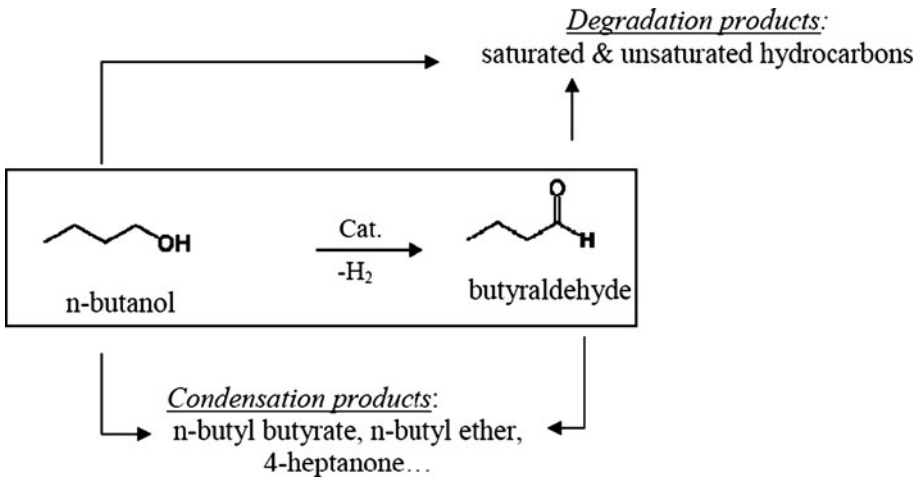

Fig. 3 Simplified scheme reaction of *n*-butanol dehydrogenation

carbonaceous species deposited on the different catalysts, it was observed that the $2Ru5Cu/ZrO_2$ catalysts had more carbonaceous deposits than their $2Ru/ZrO_2$ and $5Cu/ZrO_2$ counterparts. According to this, the interaction between Ru and Cu in the bimetallic catalyst increased carbon deposition. After only 7 h on stream, the amount of coke is higher than for $5Cu/ZrO_2$ after 29 h on stream. The catalyst with the lowest coke deposition was the catalyst supported on CeO_2.

Regarding atomic surface ratios for calcined and spent catalysts, the $5Cu/CeO_2$ catalyst showed a high Cu species surface exposure as compared to $5Cu/TiO_2$ and $5Cu/ZrO_2$ catalysts, where the Cu/M atomic ratio tends to decrease after their use in the activity tests. This fact can be attributed to surface Cu species sintering under reaction conditions. A similar behaviour was observed for the bimetallic catalyst.

3.2 Catalytic Activity

The catalytic activity tests showed that *n*-butanol conversion led to the formation of products that at room temperature can be separated into two phases: gas and liquid. The main products in the liquid phase were butyraldehyde, *n*-butyl-ether, 4-heptanone and *n*-butyl-butyrate. Traces of other products were also detected, but they were ignored due to their low concentration. In the gas phase, H_2 was the major component, although other compounds such as CO, CO_2, CH_4 and saturated and unsaturated hydrocarbons (C_3 and C_4) were also identified. The carbon balance error was less than 10% in all the activity tests.

Figure 3 presents a scheme reaction of *n*-butanol dehydrogenation. The formation of butyraldehyde is due to the dehydrogenation of *n*-butanol; at the same time, this butyraldehyde reacts with *n*-butanol to produce condensation products such as butyraldehyde, *n*-butyl-ether, 4-heptanone and *n*-butyl-butyrate. In addition, other degradation products, such as saturated and unsaturated hydrocarbons, can be produced, especially at high temperatures.

First, the activity of the bare supports was measured during 7 h on stream. For these experiments, the *n*-butanol conversions obtained were lower than 10%. These results suggest that the supports had little influence on *n*-butanol conversion under the conditions studied. The influence of the metal on monometallic and bimetallic catalyst activity is shown in Fig. 4. Among the monometallic Cu-supported catalysts, the $5Cu/ZrO_2$ catalyst provided high *n*-butanol conversion and stability during the time on stream. The conversion obtained using $5Cu/CeO_2$ or $5Cu/TiO_2$ catalysts is below 20%. Nevertheless, the conversion obtained with the $5Cu/CeO_2$ catalyst remains almost constant during the time on stream, while the $5Cu/TiO_2$ catalyst undergoes a slight deactivation after 10 h. The $2Ru/ZrO_2$ catalyst underwent fast deactivation compared with the Cu/CeO_2

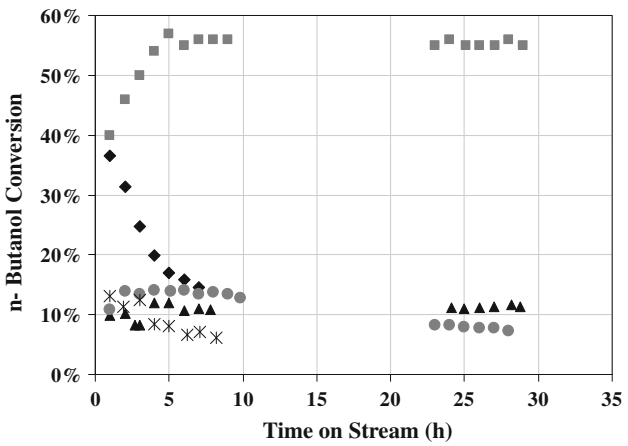

Fig. 4 Catalytic activity results for Cu, Ru and Ru–Cu supported catalysts obtained at 0.1 MPa, 648 K and with 0.1 mL/min of *n*-butanol (*filled square* $5Cu/ZrO_2$, *filled triangle* $5Cu/CeO_2$, *filled circle* $5Cu/TiO_2$, *asterisk* $2Ru/ZrO_2$, *filled diamond* $2Ru5Cu/ZrO_2$)

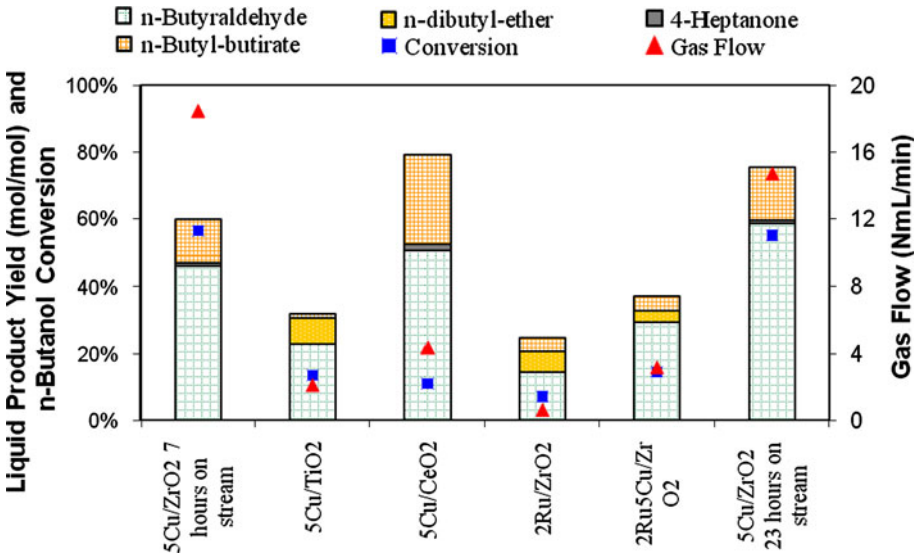

Fig. 5 *n*-Butanol conversion and the main liquid product yields (in dry basis) for Cu, Ru and Ru–Cu supported catalysts obtained at 0.1 MPa, 648 K and with 0.1 mL/min of *n*-butanol (7 h)

catalyst. This observation indicates that the Cu phases are more active and stable than the Ru ones.

Figure 5 shows the yield toward the main liquid products per mole of converted *n*-butanol, gas flow produced and *n*-butanol conversion for all the catalysts after 7 h on stream. The $5Cu/ZrO_2$ and $5Cu/CeO_2$ catalysts provided a similar butyraldehyde yield per mole of converted n-butanol, although the $5Cu/ZrO_2$ catalyst recorded a higher conversion. This finding is due to the higher gas flow produced for the $5Cu/ZrO_2$ catalysts. The formation of gaseous compounds may be a consequence of the catalytic hydrogenolysis or catalytic cracking of condensation products, such as 4-heptanone and *n*-butyl-butyrate. Nevertheless, with a higher reaction time (23 h on stream), the $5Cu/ZrO_2$ had more dehydrogenation products (butyraldehyde and butyl-ether) than $5Cu/CeO_2$ after 7 h on stream. This effect was probably due to the lower activity toward the hydrogenolysis reaction or cracking associated with gas product formation. This was consistent with the lower gas flow measured.

The liquid product yield obtained for the $2Ru/ZrO_2$ and $5Cu/TiO_2$ catalysts was low due to their poor activity. The addition of Ru to the $5Cu/ZrO_2$ catalyst reduced their activity and liquid product yield. Thus, a promoting effect was not observed. However, butyraldehyde yield still has a significant value (31%) when compared with the $5Cu/ZrO_2$ yield (45.7%).

Due to the high stability (see Fig. 4) and high butyraldehyde yield (see Fig. 5) provided by the $5Cu/CeO_2$ catalyst, the reaction temperature was increased in order to analyze the thermal behaviour of this catalyst. Therefore, Fig. 6 shows the *n*-butanol conversions at different temperatures for the $5Cu/CeO_2$ catalyst. The results indicate the need to increase the temperature to 748 K in order to obtain a 55% *n*-butanol conversion. In addition, the $5Cu/CeO_2$ catalyst remained stable at 648 and 698 K, while at 748 K a rapid deactivation of this catalyst was observed. Higher temperatures were not tested because of catalyst deactivation.

Figure 7 presents the product distribution liquid yields of the main product and by-products at the different temperatures. As can also be observed in this figure for the $5Cu/CeO_2$ catalyst, higher liquid product yield, higher gas flow and higher *n*-butanol conversion were measured at the highest temperature. The total gas flow obtained was higher for the $5Cu/CeO_2$ catalyst, indicating that, as is to be expected, cracking reactions were favoured at high temperatures. At the same time, the butyraldehyde and 4-heptanone yields increased and butyl-butyrate yield decreased;

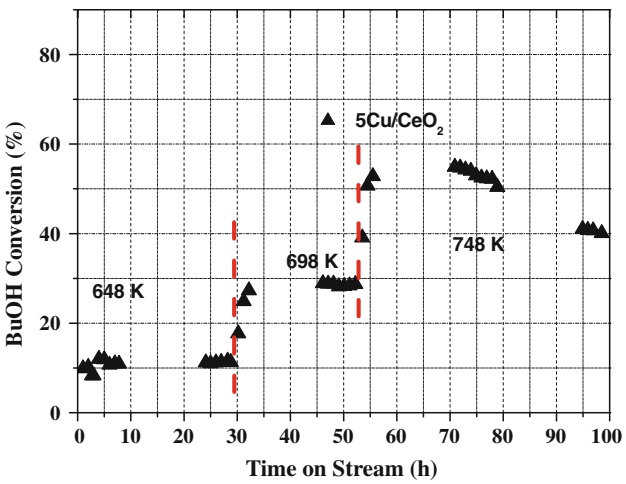

Fig. 6 Long-term activity results for the $5Cu/CeO_2$ (648, 698 and 748 K) (*filled triangle*) catalysts at 0.1 MPa and with 0.1 mL/min of *n*-butanol

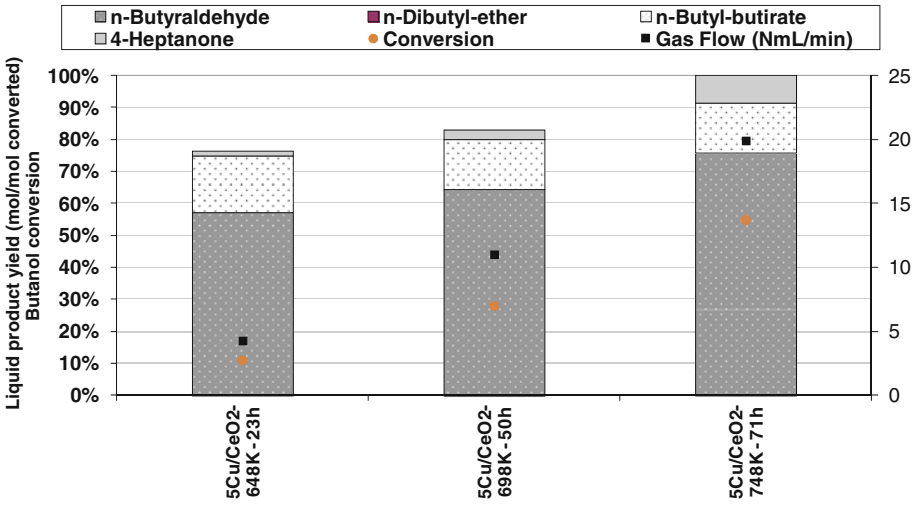

Fig. 7 *n*-Butanol conversion and the main liquid product yields (in dry basis) for the 5Cu/CeO_2 obtained at 0.1 MPa, different temperatures and time on stream

unfortunately, however, at this temperature (748 K) catalyst activity decreased rapidly with time on stream.

4 Discussion

The difference between the nominal and real copper contents in copper catalysts seems to be related to different supports. Yet the amount of copper was more or less similar in all of them. On the other hand, in the ruthenium case a low amount of ruthenium was incorporated compared to the nominal one. This could be due not only to the preparation method but also to the presence of volatile RuO_4 on the catalytic surface (XPS). It seems that the formation of this RuO_4 took place during the calcination step, and this could explain the low amount of ruthenium detected.

The supports used played an important role in catalytic activity and the liquid product yields of the monometallic Cu catalysts. The 5Cu/ZrO_2 recorded the best catalytic activity and provided a high butyraldehyde yield with a stable activity for the time on stream studied. It should be noted that the ZrO_2 support had the best textural properties (see Table 2). Although Cu incorporation reduced the ZrO_2 support's BET surface area, the 5Cu/ZrO_2 catalyst had a higher specific area than the ones measured for the 5Cu/CeO_2 and 5Cu/TiO_2 catalysts.

The 5Cu/CeO_2 and 5Cu/TiO_2 catalysts recorded lower catalytic activity than the 5Cu/ZrO_2 catalyst under the same operating conditions. After catalyst reduction, only Cu° species were detected in the 5Cu/CeO_2 and 5Cu/TiO_2 catalysts by XRD. No reflexion lines associated to Cu° and Ru° were detected for the 5Cu/ZrO_2 and 2Ru5Cu/ZrO_2 catalysts, suggesting that these species are well dispersed. In these catalysts (ZrO_2 supported), Cu appeared as Cu° after the activity test due to some sintering. The Cu reduced state was maintained in these catalysts after activity measurements.

The XPS results show that only Cu and Ru oxides were detected in the oxidation step, whilst only metallic species were detected after the reduction step and the catalysts' use in the dehydrogenation reaction. As the total reduction of Cu and Ru oxides is expected after the reduction step, it seems these metallic species withstood the dehydrogenation conditions. The ZrO_2, CeO_2 and TiO_2 species presented the same oxidation state before and after dehydrogenation. Regarding the Cu/M atomic surface ratio and chemical analysis data (see Table 1), the calcined 5Cu/ZrO_2 catalyst had a low metal surface exposure and high metal content as compared to the ones determined for the 5Cu/CeO_2 and 5Cu/TiO_2 catalysts. These observations suggest that most of the Cu species were inside the ZrO_2 porous structure in the 5Cu/ZrO_2 catalyst. In addition to this, Cu particles were not detected by XRD in this catalyst. Apart from a good dispersion, this observation proves that Cu species were incorporated into the support structure.

The effect described above was not detected for the 5Cu/CeO_2 and 5Cu/TiO_2 catalysts. These catalysts had higher Cu surface exposure but lower activity than the 5Cu/ZrO_2 catalyst. Therefore, the catalytic activity and stability shown by the 5Cu/ZrO_2 catalyst in n-butanol dehydrogenation seems to be in accordance with the incorporation of well dispersed Cu species inside the ZrO_2 porous structure.

On the other hand, the reduced 5Cu/CeO_2 and 5Cu/TiO_2 catalysts recorded a greater average particle size for the Cu° than the reduced 5Cu/ZrO_2 catalyst, indicating that these particles underwent agglomeration phenomena. This fact contributed to the low activity measured for the 5Cu/CeO_2 and 5Cu/TiO_2 catalysts in the dehydrogenation reaction.

As the Cu/Al atomic surface ratio differences between calcined and reduced catalysts have shown (see Table 1),

Cu-supported catalysts generally underwent a reduction in Cu° exposure. Considering that XPS is a surface technique, sintering may occur in the surface Cu° species, while the Cu° species deposited inside the support structure maintained their good dispersion in the $5Cu/ZrO_2$ catalyst. XPS also revealed that carbon deposition took place during *n*-butanol dehydrogenation. This carbon formation can be associated to cracking reactions (Table 1).

$5Cu/CeO_2$ recorded a higher initial butyraldehyde yield (51.3%) than the most active catalyst $5Cu/ZrO_2$ (after 7 h), although after 23 h on stream (Fig. 5, 7) $5Cu/ZrO_2$ presented a slightly higher butyraldehyde yield than $5Cu/CeO_2$. This higher butyraldehyde yield corresponded to a lower gas flow. The formations of gaseous compounds-a consequence of the catalytic hydrogenolysis or catalytic cracking of condensation products-are usually promoted by acid centres. The presence of coke in this catalyst deactivates the acid centres, decreasing gas production and increasing the dehydrogenation product yields as butyraldehyde and butyl butyrate. The activity results are in close agreement with this explanation (Fig. 5). Using this catalyst when temperature was increased, both conversion and butyraldehyde yield reached higher values. The synergistic effect between the metals and CeO_2 might be responsible for this improvement. Pre-treatment of the catalysts by hydrogen caused a partial reduction in ceria and thus led to the generation of Ce^{3+} species on the catalyst surface (TPR). The Ce^{3+} species enhanced the adsorption of alcohols through the coordination between the Ce^{3+} cation and the hydroxyl group, which favours the dehydrogenation of alcohols [27]. Unfortunately, however, the catalyst was deactivated very quickly at 748 K. This fact can be related to the higher loss of surface Cu° exposure at 748 K (XPS) but not to coking, as $5Cu/CeO_2$ was the catalyst with the lowest tendency to coke production (Table 1). This good behaviour may be attributed to the oxygen mobility of the CeO_2.

The $2Ru/ZrO_2$ catalyst recorded lower activity than the $5Cu/ZrO_2$ catalyst. The low initial conversion decreased during time on stream. After 7 h, conversion decreased from 12 to 5%. This can be related to metal sintering because low carbon content was found on the catalytic surface (Table 1). In addition, low metal content could be the main influence on the activity measured. Although, the bimetallic $2Ru5Cu/ZrO_2$ catalyst registered good initial activity, it was quickly deactivated during the initial time on stream (Fig. 4). This finding could be attributed to the second metal incorporation blocking the Cu previously deposited on the ZrO_2 pore structure, and also to a reduction in the interaction between the CuO crystallites and the support, as the BET surface area and the TPR profiles reflected. This weaker interaction might facilitate Cu and Ru particle sintering (XPS). This result was confirmed by the coke deposition after only 7 h on stream (Table 1). The highest coke deposition was reached for the bimetallic catalyst. Large metal particles are required for coke deposition, hence it seems the presence of Ru favours metal sintering, increasing both particles size and coke deposition.

5 Conclusions

The activity measurements carried out on the $5Cu/ZrO_2$ catalyst revealed it has a promising activity and stability for *n*-butanol dehydrogenation to butyraldehyde. These properties are related to a good dispersion of the Cu active phases inside the ZrO_2 pore structure. The $5Cu/CeO_2$ and $5Cu/TiO_2$ catalysts provided lower *n*-butanol conversions than the $5Cu/ZrO_2$ catalyst under the same operating conditions. This can be attributed to the incorporation of Cu species mainly on the external surface of the catalysts. Nevertheless, the $5Cu/CeO_2$ catalyst registered acceptable stability and a high butyraldehyde yield, with *n*-butanol conversion and butyraldehyde yield increasing with temperature. The synergistic effect between the metals and CeO_2 might be responsible for this improvement. However, $5Cu/CeO_2$ registers major deactivation problems at high temperature, which may be related to high metal sintering.

Ru incorporation to $5Cu/ZrO_2$ reduced this catalyst's activity, stability and butyraldehyde yield. This behaviour can be related to the Ru presence weakening the Cu-support interaction. These weaker interactions could favour metal sintering, coke deposition and, as a result, catalyst deactivation.

Acknowledgments The authors gratefully acknowledge the financial support for this work provided by the Spanish Ministry of Science and Technology (ENE2010-21198-C04-03) and the University of the Basque Country, and the Instituto de Catálisis y Petroleoquímica (ICP-CSIC) for its help in catalyst characterization.

References

1. Shiau C-Y, Liaw S-T (1990) J Chin I Ch E 21:85–92
2. Shiau C-Y, Liaw S-T, Chem J (1992) Technol Biotechnol 53:13–19
3. Raizada K, Tripathi VS, Lal D, Singh GS, Dwivedi CD (1996) J Chem Technol Biotechnol 56:265–270
4. Shiau C-Y, Tsai JC (1998) J Chem Technol Biotechnol 73:414–420
5. Basinska A, Klimkiewicz R, Domka F (2001) Appl Catal Gen 207:287–294
6. Adam F, Andromena I (2009) J Porous Mater 16:321–329
7. Caputo T, Lisi L, Pirone R, Russo G (2008) Appl Catal Gen 348:42–53
8. Boccuzzi F, Chiorino A, Martra G, Gargano M, Ravasio N, Carrozzinni B (1997) J Catal 165:129–139
9. Mitsui T, Tsutsui K, Matsui T, Kikuchi R, Eguchi K (2008) Appl Catal B 81:56–63

10. Zonetti P, Landers R, Gomez Cobo AJ (2008) Appl Surf Sci 254:6849–6853
11. Reyes P, König ME, Pecchi G, Granados ML, Fierro JLG (1997) Catal Lett 46:71–75
12. Lanza R, Järas SG, Canu P (2007) Appl Catal Gen 325:57–67
13. Ali MA, Kimura T, Suzuki Y, Al-Saleh MA, Hamid H, Inui T (2002) Appl Catal Gen 277:63–72
14. Li L, Qu L, Cheng J, Li J, Hao Z (2009) Appl Catal 88:224–231
15. Profeti LPR, Ticianelli EA, Assaf EM (2009) Int J Hydrogen Energy 34:5049–5060
16. Ritzkopf I, Vukojevic S, Weidenthaler C, Grunwaldt J-D, Schüth F (2006) Appl Catal Gen 302:215–223
17. Kundakovic Lj, Flytzani-Stephanopoulos M (1998) Appl Catal Gen 171:13–29
18. Iriondo A, Barrio VL, Cambra JF, Arias PL, Güemez MB, Sanchez-Sanchez MC, Navarro RM, Fierro JLG (2010) Int J Hydrogen Energy 35:11622–11633
19. Requies J, Rabe S, Vogel F, Truong T-B, Filonova K, Barrio VL, Cambra JF, Güemez MB, Arias PL (2009) Catal Today 143:9–16
20. González ID, Navarro RM, Álvarez-Galván MC, Rosa F, Fierro JLG (2008) Catal Commun 9:1759–1765
21. Ma L, He D, Li Z (2008) Catal Commun 9:2489–2495
22. John FM, William FS, Peter ES, Kenneth DB (1995) Handbook of X-ray photoelectron spectroscopy. Physical Electronics, Inc., Minnesota USA
23. Chan HYH, Takoudis CG, Weaver MJ (1997) J Catal 172:336–345
24. Hamwi A, Latouche C, Dupuis J, Benoit R, Marchand V (1996) J Phys Chem Solids 57:991–998
25. Serrano DP, Botas JA, Fierro JLG, Guil-López R, Pizarro P, Gómez G (2010) Fuel 89:1241–1248
26. Moreno-Castilla C, López-Ramón MV, Carrasco-Marín F (2000) Carbon 38:1995–2001
27. Wei S, Ruijuan S, Junlong L, Ensheng Z, Zhanshuang L, Yide X, Wenjie S (2007) Chin J Catal 28(2):106–108